Energy 304 (2024) 132186

Contents lists available at ScienceDirect

Energy

journal homepage: www.elsevier.com/locate/energy

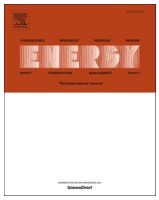

Water transport across the membrane of a direct toluene electro-hydrogenation electrolyzer: Experiments and modelling

Antonio Atienza-Márquez [a,b,*], Shota Oi [c], Takuto Araki [d], Shigenori Mitsushima [b,e]

[a] Universidad de Málaga, Energy Research Group (GEUMA), C/ Doctor Ortiz Ramos s/n, Málaga, 29071, Spain
[b] Yokohama National University, Institute of Advanced Sciences (IAS), Tokiwadai 79-5, Hodogaya-ku, Yokohama, 240-8501, Japan
[c] Yokohama National University, Graduate School of Engineering Science, Tokiwadai 79-5, Hodogaya-ku, Yokohama, 240-8501, Japan
[d] Yokohama National University, Faculty of Engineering, Division of Systems Research, 79-5, Hodogaya-ku, Yokohama, 240-8501, Japan
[e] Yokohama National University, Green Hydrogen Research Center, 79-5, Hodogaya-ku, Yokohama, 240-8501, Japan

ARTICLE INFO

Handling Editor: Henrik Lund

Keywords:
Water mass transport
Hydrogen energy technologies
Toluene/MCH organic hydride
Electrolyzer
Polymeric electrolyte membrane
Electro-osmosis

ABSTRACT

Toluene/methylcyclohexane is a promising liquid organic hydride for hydrogen storage and transport under ambient conditions. Direct toluene electro-hydrogenation electrolyzers, utilizing proton exchange membrane technology, offer benefits in reducing the reversible decomposition voltage and eliminating theoretical heat losses associated with conventional hydrogenation methods. Nevertheless, water transport across the membrane can inhibit the supply of toluene to reaction sites at the cathode. This study investigates water transport across the Nafion™ 117 membrane of an in-house electrolyzer cell, employing sulfuric acid and toluene solutions as the anode and cathode reactant, respectively, and operating at current densities from 0.1 to 0.8 A/cm^2. The experiments show that the cathode toluene concentration has a negligible effect on drag water, while water flux increases with electric current and decreases with higher anode sulfuric acid concentrations. The modelling approach assumes electro-osmosis and diffusion mechanisms govern water transport. Simulations predict a linear decrease in the electro-osmotic drag coefficient from 2.3 to 1.6 as the sulfuric acid concentration rises from 0.1 to 1.5 mol/L, while the back diffusion flux increases linearly up to 2 mg/(min·cm^2). These findings closely align with experimental data and previous literature, despite the high complexity of water transport in polymer electrolyte membranes.

1. Introduction

Decarbonization requires a greater penetration of renewable energy sources and a reduced reliance on fossil fuels. However, renewables face bottlenecks such as intermittent generation and uneven geographic distribution, which can make direct electrification difficult in some locations [1]. This requires the development of technologies for the storage and large-scale transport of green electricity. Green hydrogen is a promising renewable energy carrier for long-haul transport [2].

However, hydrogen is a gas at ambient conditions and has a very low volumetric energy density (e.g., 0.003 kWh/L, compared to gasoline's 8.6 kWh/L [3]), making it challenging to store and transport [4]. Among the numerous existing hydrogen storage technologies (e.g., compressed [5], liquefied hydrogen [6], metal hydrides [7], and so forth), liquid organic hydrogen carriers (LOHCs) are a type of organic hydride that enables storage and transport of hydrogen in the liquid phase at ambient temperature and pressure [8]. Fig. 1 illustrates the basic working principle of LOHCs, which reversibly bind hydrogen (hydrogenation) and release hydrogen (dehydrogenation) to and from a carbon-based molecule [9]. LOHC technology present a promising alternative to, for example, deep ocean pipelines [10], and offers potential solution for international maritime hydrogen trade [11,12]. Thus, LOHCs may play a key role in a global renewable energy market. Their integration into polygeneration schemes and distributed energy networks could enable a more efficient and flexible energy system, fostering sector coupling [13].

Despite the existence of multiple LOHC candidates, none are ideal in terms of storage capacity, dehydrogenation energy for hydrogen release, safety, and cost [14]. For example, the naphthalene/decalin system has good hydrogen storage capacity (2.2 kWh/L), but it risks solidification at ambient temperature [15], which can damage pipes, valves, and other accessories. The benzene/cyclohexane pair also has an acceptable hydrogen content (1.86 kWh/L), but benzene is a known carcinogen

* Corresponding author. Universidad de Málaga, Energy Research Group (GEUMA), C/ Doctor Ortiz Ramos s/n, Málaga, 29071, Spain.
E-mail address: atienza-marquez@uma.es (A. Atienza-Márquez).

https://doi.org/10.1016/j.energy.2024.132186
Received 3 November 2023; Received in revised form 24 May 2024; Accepted 22 June 2024
Available online 24 June 2024
0360-5442/© 2024 The Authors. Published by Elsevier Ltd. This is an open access article under the CC BY-NC-ND license (http://creativecommons.org/licenses/by-nc-nd/4.0/).

[16]. While the toluene/methylcyclohexane (MCH) system has high dehydrogenation energy and temperature and a lower volumetric hydrogen storage capacity than other hydrogen carriers, such as liquid hydrogen or ammonia, it is an easily manageable and stable liquid over a wide temperature range (−95–111 °C) [17]. Additionally, toluene has low toxicity and gasoline-like properties, allowing the use of existing oil infrastructure [18].

Fig. 1 also shows that direct toluene hydrogenation is a promising alternative to conventional toluene hydrogenation, which relies on a two-step process (electrolysis followed by hydrogenation in a chemical reactor). As shown in Fig. 2, direct toluene hydrogenation occurs in a single step using proton exchange membrane (PEM) electrolyzer technology. This avoids the thermal losses associated with the conventional process (Fig. 1) and has a lower theoretical voltage than electrochemical water splitting (1.08 V vs. 1.23 V, respectively [19]). Therefore, direct toluene hydrogenation could improve energy efficiency compared to conventional toluene hydrogenation [20]. Direct toluene electro-hydrogenation electrolyzers operate by splitting water at the anode electrode to produce protons, electrons, and oxygen. The protons migrate through the polymeric electrolyte membrane to the cathode catalyst layer, where they react with the transferred electrons and the toluene transported through the porous transport layer to produce MCH. The following reactions occur simultaneously at both electrodes [21]:

$$\text{Anode}: 2\,H_2O \rightarrow O_2 + 4\,H^+ + 4\,e^- \quad (1\text{-}1)$$

$$\textit{Cathode}: C_7H_8 + 6\,H^+ + 6\,e^- \rightarrow C_7H_{14} \quad (1\text{–}2)$$

However, the overall conversion ratio can be lower than 100 % in practice. Previous research on direct toluene electro-hydrogenation electrolyzers has focused on improving the electrochemical performance of this technology by studying the effects of the following factors [22]: Geometry of the flow field plates [19], operating temperature and toluene concentration [23], type of membrane [21], catalyst material [24,25] and thickness of the catalyst layer [20]. Recent studies have also visualized water droplets, and hydrogen bubbles on the cathode porous transport layer (PTL) and hydrogen bubbles inside the PTL for the first time [14,18], with the aim to understand their behavior and distribution. Regarding private initiatives, ENEOS corporation [26] currently develops direct toluene electro-hydrogenation technology under the name Direct-MCH®. In 2023, the Japanese company built a demo plant in Australia featuring a 150-kW electrolyzer unit [27]. Their deployment roadmap continues towards megawatt-scale and commercialization.

A research gap exists on a critical technical issue affecting the efficiency of direct toluene electro-hydrogenation electrolyzers: the transport of water across the proton-conducting membrane. As shown in Fig. 2, water dragged across the membrane from the anode side may obstruct the toluene transport pathway to the reaction sites. Consequently, toluene supply to the cathode catalyst layer may be insufficient, resulting in hydrogen gas generation as a side reaction. Thus, while membrane hydration is essential for proton conductivity [28], water transport across the membrane must be controlled. In fact, water management plays a pivotal role in electrochemical devices. Numerous studies in proton exchange membrane fuel cell (PEMFC) technology have investigated the water mass transport within catalyst layers [29], gas diffusion layers [30] and across perfluorinated sulfonic-acid (PFSA) membranes (e.g., Nafion™) [31]. This paper focuses on the latter case, for the first time within the context of direct toluene electro-hydrogenation electrolyzer technology.

The water transport across PFSA membranes is extremely complex, involving multiple mechanisms and is not fully understood [32]. The published data emphasize the uncertainty of the phenomenon [33]. For example, pressure, temperature, and concentration gradients can drive water transport, and protons migrating through the membrane can drag water molecules along with them [31], which are then discharged at the cathode. Besides, the understanding of water transport becomes notably intricate when employing a sulfuric acid solution as the anode reactant, as illustrated in Fig. 2. This approach, widely adopted in industrial electrolyzers with dimensionally stable electrode (DSE®) technology for oxygen evolution, relies on the stability of sulfuric acid's anions and its proton source capacity, thereby promoting the electrolysis process [34,35]. Sulfuric acid induces concentration gradients between both sides of the polymeric electrolyte membrane, which impacts water transport through the membrane. Yet this aspect remains unexplored in direct toluene electro-hydrogenation electrolyzers.

Considering the above-mentioned gaps of knowledge, this work presents an investigation that combines experiments and modelling to study the water transport across the polymeric electrolyte membrane of an operational direct toluene electro-hydrogenation electrolyzer cell. The experimental results are first analyzed to understand the phenomena under different operating conditions. Subsequently, these results are used to develop a model characterized by its simplicity and minimal number of parameters.

2. Experimental and modelling

2.1. Experimental setup

Fig. 3 (a) shows the structure of the toluene direct toluene electro-hydrogenation electrolyzer used in this study, and Fig. 3 (b) shows a picture of the in-house cell developed. The anode's end plate consists of a rib-and-channel flow field plate which leads to a parallel flow configuration in the height direction of the electrolyzer and improve the

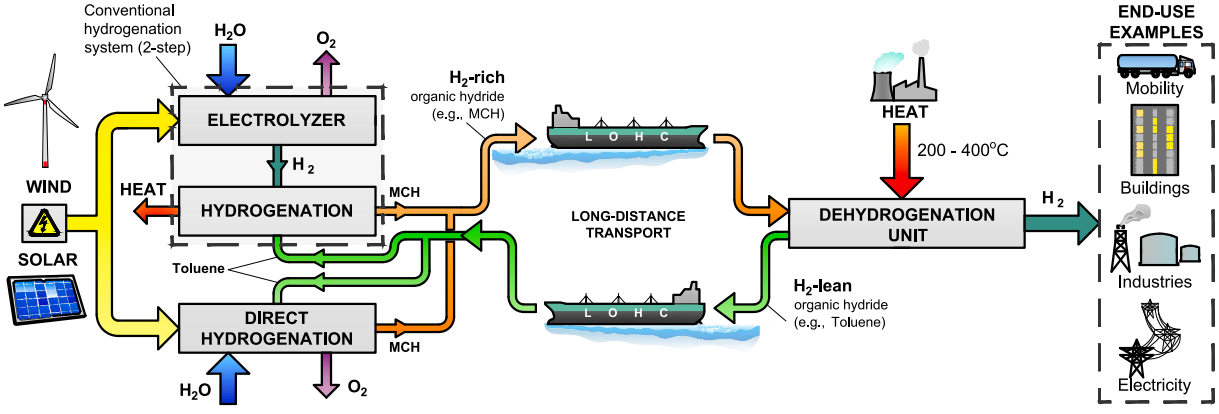

Fig. 1. Schematic diagram of the conversion of renewable electricity to green hydrogen, its long-distance transport via the hydrogenation (conventional or direct method) and dehydrogenation of a liquid organic energy carrier (LOHC), and its utilization at the point of demand. (For interpretation of the references to colour in this figure legend, the reader is referred to the Web version of this article.)

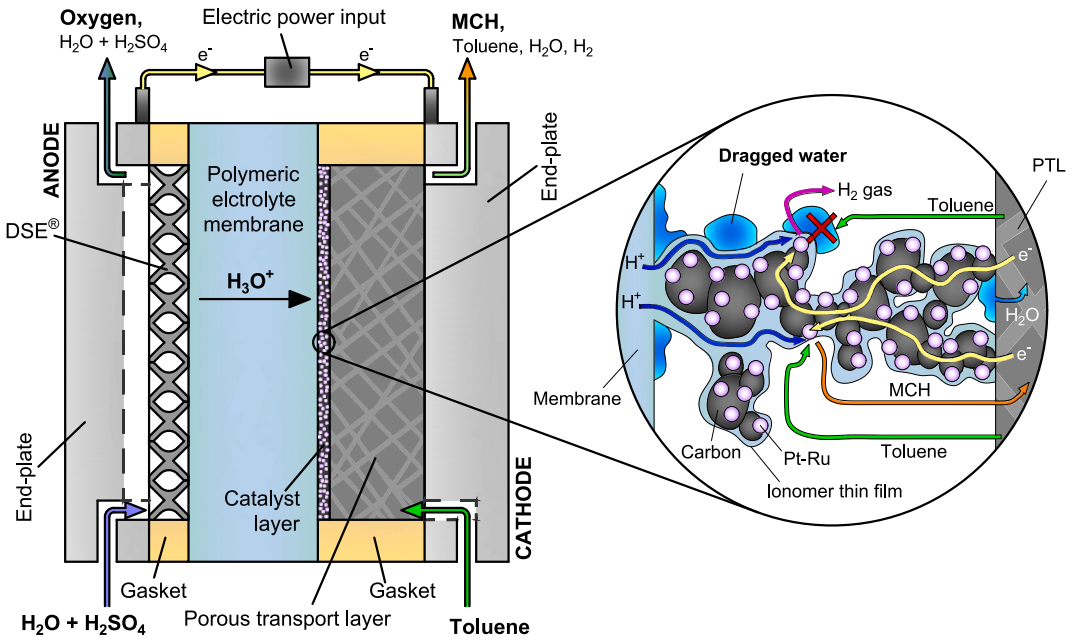

Fig. 2. Schematic diagram of a direct toluene electro-hydrogenation cell.

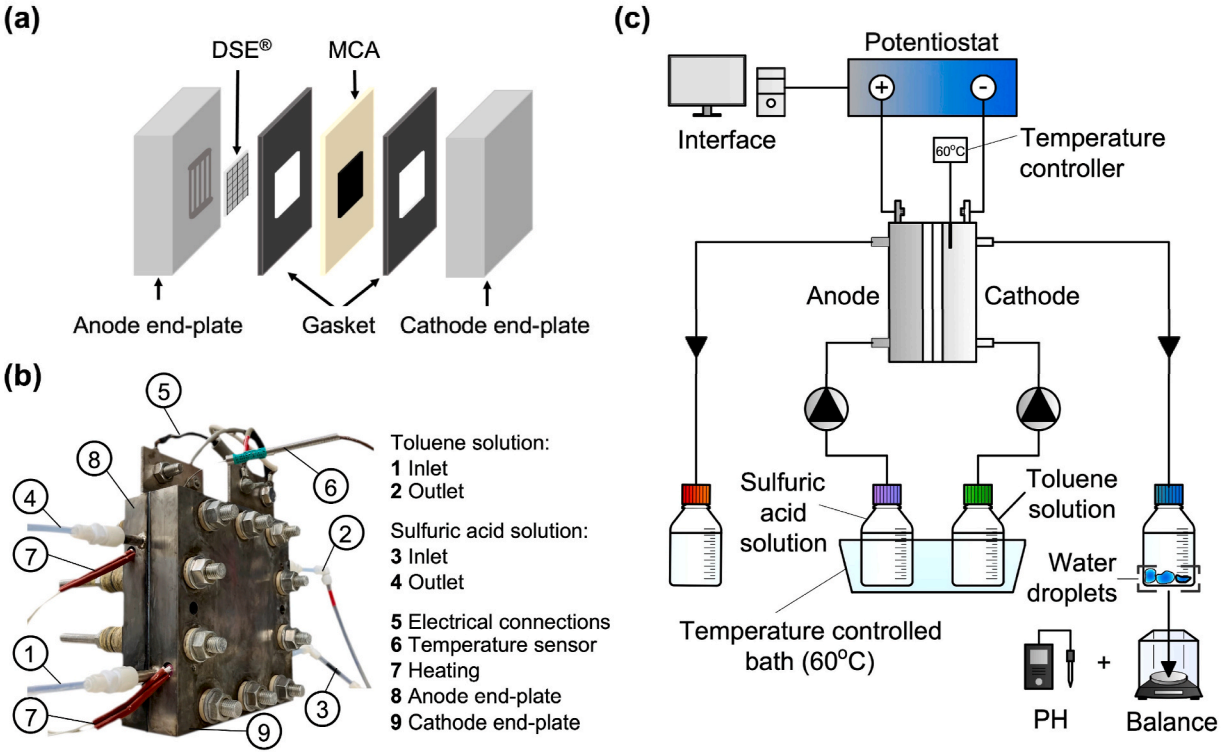

Fig. 3. Direct toluene electro-hydrogenation electrolyzer developed in this study. (a) Main components. (b) Photograph. (c) Schematic diagram of the experimental setup.

escape of oxygen bubbles generated at the electrode. As for the cathode side, a flat flow field end plate was used. To avoid fluid leakages, a gasket was placed between the membrane and the titanium end plates on both the anode and cathode sides, and the anode was pressed against the membrane. The anode is based on industrial electrolyzers and uses DSE® technology electrode for the oxygen evolution reaction [36]. Sulfuric acid and toluene solutions were supplied as anode and cathode reactants, respectively.

The membrane cathode assembly (MCA) was prepared by sandwiching the catalyst-coated substrate (CCS) and the polymer electrolyte membrane (Fig. 3(a)). The CCS was integrated by the cathode's catalyst layer and PTL. The PTL consists of carbon paper (SGL Sigracet® 10BC [37], hydrophobic) loaded with 0.02 mg/cm^2 of Pt nanoparticles to enhance the indirect hydrogenation of toluene, utilizing the hydrogen gas generated as a byproduct from a side reaction within the cathode catalyst layer. In the preparation of the catalyst layer, Pt–Ru/C powder (TEC61E54, Tanaka Kikinzoku Kogyo [38]) was blended with a perfluoro-sulfonic acid (PFSA) polymer dispersion of 5 wt% ionomer

(Nafion™, Dupont) and using 1-propanol as a solvent. This mixture was then subjected to ball milling for 30 min at 300 rpm, employing 15 zirconia balls with a 3 mm diameter. Subsequently, using a bar-coater and a 0.45 mm-thick aluminum mask, the mixed ink was applied into the microporous layer side of the PTL serving as the porous substrate material. The resulting catalyst (Pt–Ru) loading and active area were 0.669 mg/cm^2 and 10 × 10 cm^2, respectively. Finally, the perfluorinated sulfonic-acid membrane (Nafion™ 117) and the CCS were bonded by hot pressing at 120 °C and 4 MPa for 3 min.

Fig. 3(c) shows the schematic diagram of the experimental system, whose operation is as follows. Toluene was supplied to the cathode side at 100 and 10 vol% on dilution with MCH to represent the bottom and upper position of the cathode side in a large-scale electrolyzer. On the other hand, the concentrations of sulfuric acid considered in the anode reactant were 0.1, 0.5, 1.0 and 1.5 mol/L. Regarding the electric current, the electrolyzer cell operated within the range of 0.1–0.4 A/cm^2, with increments of 0.1 A/cm^2, for the case of 10 % toluene in the cathode reactant. For the scenario with toluene concentration at 100 % in the cathode reactant, the operation covered the range of 0.2–0.8 A/cm^2, with increments of 0.2 A/cm^2. Table 1 summarizes the operating conditions and the main features of the electrolyzer cell.

The following experimental procedure was implemented to quantify the transported water across the membrane. Initially, a pretreatment phase (2 h) was undertaken to enhance the stability of both water content and the proton conduction pathway within the electrolyte membrane. This pretreatment also aimed to mitigate potential irregularities in the sulfuric acid concentration distribution across the membrane, ensuring uniformity, and establishing a consistent electrocatalyst performance during the initial break-in period. The pretreatment protocol consisted of two sequential stages. The initial stage involves membrane swelling, where diluted sulfuric acid and toluene solution were separately supplied to the anode and cathode sides. This phase occurred under open-circuit conditions at 60 °C for a duration of 1 h. Following this, an electric current was applied at a rate of 0.4 A/cm^2 for 1 h. The pretreatment protocol was executed at the beginning of each experimental set, determined by a given concentration of sulfuric acid or toluene in the anode or cathode reactant, respectively.

After the pretreatment, air was introduced into both the anode and cathode sides to facilitate pipe drainage. Next, the concentrations of sulfuric acid and toluene at the anode and cathode reactants, respectively, were adjusted, and the system was operated in recirculation mode for 20 min before electrolysis. This step was taken to maintain the water permeation rate at equilibrium conditions consistent with the pretreatment stage, despite the minimal water permeation through the membrane under open circuit conditions. Afterward, a constant electric current density was applied for 20 min, and the fluid stream exiting the cathode was collected. Because water droplets are immiscible with the oil phase (i.e., toluene and MCH), they can be extracted using a dropper and subsequently weighed on a balance. After measuring the water quantity for all the electric current densities investigated, the entire experimental process was replicated for the other sulfuric acid and toluene concentrations considered in this work.

Table 1
Electrolyzer characteristics and experimental conditions.

Parameter	Value
Catalyst weight ratio ionomer/Carbon	0.8:1.0
Cathode catalyst (Pt–Ru) loading	0.669 mg/cm^2
Cathode porous transport layer	SGL 10BC+ 0.02 mg-Pt/cm^2
Active area	10 × 10 cm^2
Toluene supply (cathode), ratio to MCH	10, 100 vol%
H_2SO_4 concentration at anode's reactant	0.1, 0.5, 1.0, 1.5 mol/L
Cell operating temperature	60 °C
Current density range	0.1–0.8 A/cm^2
Cathode flow rate (toluene solution)	10 mL/min
Anode flow rate (sulfuric acid solution)	10 mL/min

Sulfuric acid crossover. Cation exchange membrane prevents anion transportation, but small amount of sulfate anion in anolyte also permeates the membrane influencing water transport. To assess the amount of sulfuric acid permeating the membrane, the following method was implemented. A pH meter was utilized to measure the water collected at the cathode drain, under conditions where 100 % toluene was supplied at a current density of 0.4 A/cm^2. The sulfuric acid concentration in the collected water was determined by comparing it with standard sulfuric acid solutions of known concentrations, ranging from 0.01 to 1.5 mol/L. Toluene crossover has been excluded from consideration, in line with the low permeability values reported by Nagasawa et al. [21].

2.2. Modelling

Fig. 4 depicts a schematic diagram of the water transport through the polymer electrolyte membrane of a direct toluene electro-hydrogenation electrolyzer. A one-dimensional modelling (*x*-direction) in the through-plane direction of the membrane has been developed in Python 3.12.0 [39].

The modelling assumes that the electrolyzer operates under steady-state and equilibrium conditions. The water transport across the membrane is mainly governed by electro-osmotic drag and back-diffusion mechanisms. The entire system is assumed to be maintained at a constant and uniform temperature throughout [40]. Consequently, water transport via thermo-osmosis [41] is disregarded. On the other hand, this study does not consider the water mass transport due to convection driven by pressure gradient (i.e., hydraulic permeation) [42–44]. The net water flux ($N_{w,net}$) across the membrane is computed using the following mathematical expression:

$$N_{w,net} = N_{w,EOD} + N_{w,DIF} \tag{2}$$

The electro-osmotic drag flux ($N_{w,EOD}$) is calculated as follows:

$$N_{w,EOD} = \frac{\xi \times i}{F} \tag{3}$$

where i represents the electric current density (A/m^2) and F is Faraday's constant (96 485 A s/mol). The variable ξ is the electro-osmosis coefficient and signifies the number of water molecules carried by each proton moved by an electric field through the membrane and migrating from the anode to the cathode side [32]. Despite there is a large body of literature on the estimation of ξ in perfluorinated sulfonic-acid membranes, this coefficient has been controversial due to the complex nature of coupled ion/water transport and the difficulty in measuring it [33]. Many authors have proposed correlations that establish a relationship between the electro-osmotic drag coefficient and the hydration number of the membrane [33], yet none are fully satisfying. Based on previous studies, the modelling presented in this work assumes that this

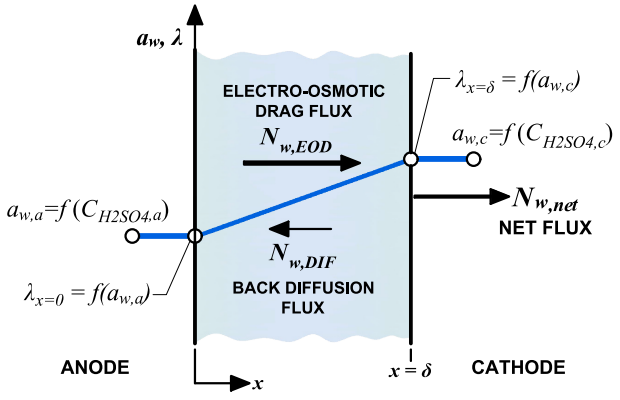

Fig. 4. One-dimensional water transport across the polymer electrolyte membrane.

coefficient is independent of the electric current density [45].

The diffusion flux ($N_{w,DIF}$) arises from the water concentration gradient ($\Delta\lambda$) between the surfaces of the Nafion™ membrane. Its mathematical expression is presented as follows [46]:

$$N_{w,DIF} = -D_{w,F} \times \frac{\rho_m}{EW} \frac{\Delta\lambda}{\Delta x} \quad (4)$$

where ρ_m and EW are the density (dry, 2 000 kg/m^3), and equivalent weight (1.1 kg/mol) of the membrane, respectively. The term $\Delta\lambda \cong \lambda_{x=\delta} - \lambda_{x=0}$ is the water content gradient between both sides of the membrane, and Δx corresponds to the thickness of the membrane (δ, 183 μm), which is assumed to remain constant regardless of the water content [47]. The membrane water content λ (mol H_2O/mol SO_3^-), whose calculation is explained in detail in **Appendix A.1**, represents the number of water molecules per mole of sulfonic acid groups in the Nafion™ [48]. For the sake of simplification, the model assumes a linear variation in water content across both sides of the membrane [49]. The coefficient $D_{w,F}$ in **Eq. (4)** is the average steady-state Fickian diffusivity of water in the membrane. Similar to the electro-osmotic mechanism, diffusion coefficient has been a source of substantial uncertainty and debate in scientific literature for many years [50].

This study does not consider interfacial water transport resistances on either side of the membrane. These resistances are effectively eliminated or minimized in membranes that have been equilibrated with a liquid phase [4,5]. Therefore, in terms of boundary conditions, the water content of the membrane at the interfaces between DSE®/membrane and membrane/cathode catalyst is computed using the thermodynamic activity of water in the bulk solution at the anode ($a_{w,a}$) and cathode ($a_{w,c}$) sides, respectively (Fig. 4).

According to the modelling assumptions, substituting Eq. (3) into Eq. (2) yields a linear relationship of the net water flux and current density. The pair ξ and $N_{w,DIF}$ are determined to minimize the error between the measured and calculated net water flux for each case of sulfuric acid concentration at the anode. Subsequently, the coefficient $D_{w,F}$ is calculated using Eq. (4).

Lastly, in order to assess the accuracy of the calculations derived from the aforementioned modeling when compared to the experimental data, we employed the normalized mean bias error (*NMBE*), defined as follows:

$$NMBE = \frac{1}{\overline{N}_{wE}} \frac{\sum_{j=1}^{n} (N_{wE,j} - N_{wC,j})}{n} \times 100\% \quad (5)$$

where N_{wE} and N_{wC} represent the measured and calculated net water flux, respectively, n is the number of experimental values measured for a given anode sulfuric acid concentration and $\overline{N}_{wE}$ denotes the arithmetic mean of the sample of n measurements.

3. Results and discussion

3.1. Experimental measurements

Fig. 5 (a) shows the total water flux measured at the cathode outlet under various operating conditions, including electric current, sulfuric acid concentration, and toluene concentration. The results show no significant difference in water flux between the 10 and 100 vol% toluene solutions. Therefore, the effect of toluene concentration on water flux across the membrane is negligible. For the simulations, the average water flux was considered for those electric current densities where water flux was measured at both toluene concentrations.

The amount of water dragged across the membrane increased with electric current and decreased with sulfuric acid concentration in the anode reactant. For instance, with a 1.5 mol/L sulfuric acid solution, the water flow decreased by 2.1 mg/(min·cm^2) and 7.7 mg/(min·cm^2) at 0.1 and 0.8 A/cm^2, respectively, compared to a 0.1 mol/L sulfuric acid solution. In relative terms, that water flux decrease was more noticeable at lower electric currents. For example, at 0.2 A/cm^2 and with a 0.1 mol/L sulfuric acid solution, the water flux decreased by 23 %, 48 %, and 68 % as the sulfuric acid concentration increased to 0.5, 1.0, and 1.5 mol/L, respectively. When the electric current was raised to 0.8 A/cm^2 under the same sulfuric acid conditions, the reductions in water flow were 8.1 %, 26.1 %, and 37.5 %. This suggests that the sulfuric acid concentration could be adjusted to control water transport depending on the operating conditions.

As depicted in Fig. 5(a), the slope of the water flux exhibits a decreasing trend as the anode's concentration of sulfuric acid increases, while the intercept with the ordinate axis shifts towards more negative values. This observation implies that, for a constant electric current, the electro-osmotic flux tends to decrease as the sulfuric acid concentration rises, while the back diffusion effect intensifies. A more detailed discussion of this phenomenon will follow in the subsequent sections.

Fig. 5(b) shows the amount of sulfuric acid measured at the cathode side for different anodic sulfuric acid concentrations at a current density of 0.4 A/cm^2 and a 100 vol% toluene solution at the cathode side. The results show that sulfate ions, as anions, also permeate the Nafion™ film. For example, the sulfuric acid concentration at the cathode outlet was 0.14 mol/L when the anodic sulfuric acid concentration was 1.5

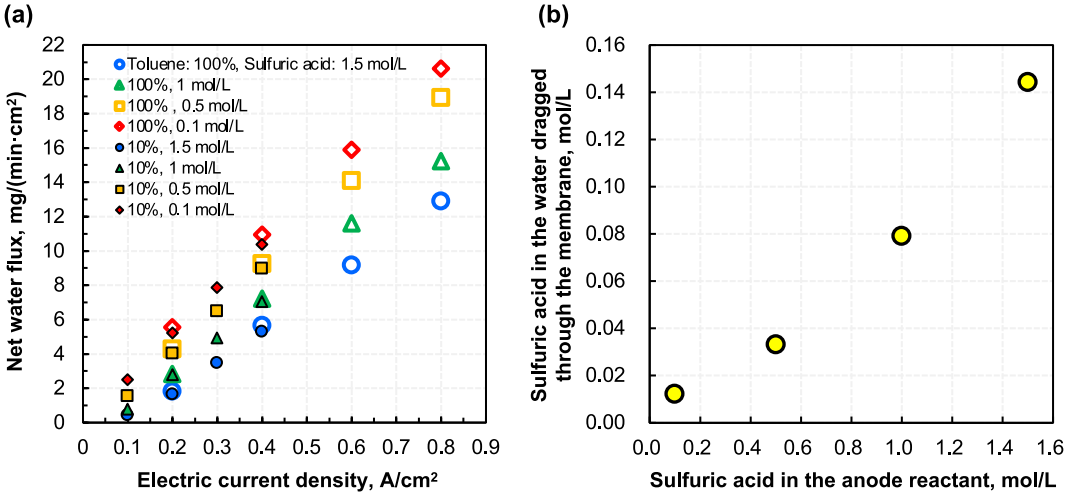

Fig. 5. Experimental measurements. (a) Net water flux as a function of electric current density and sulfuric acid concentration in the anode reactant. (b) Sulfuric acid concentration at the cathode side as a function of its concentration at the anode.

mol/L and 0.09 mol/L when the anodic sulfuric acid concentration was 0.5 mol/L. This indicates that approximately 1/10 of the sulfuric acid in the anode reactant crosses over to the cathode side, creating a concentration gradient in the membrane that drives back diffusive water flux.

Table A.1 (Appendix A) shows the thermodynamic activity of water and the water content of the membrane at the cathode and anode sides, both calculated using the method explained in **section 2.2**. The relationship between the cell potential and the current density is shown in Appendix B.

3.2. Electro-osmotic drag mechanism

Fig. 6 (a) and Table 2 shows the electro-osmotic drag coefficient that minimized the deviations between the calculated and measured net water flux. The electro-osmotic drag coefficient obtained decreases nearly linearly from 2.3 to 1.6 (mol H_2O/mol H^+) as the concentration of sulfuric acid in the anode reactant increases from 0.1 to 1.5 mol/L. Hence, the electro-osmotic drag coefficient can be estimated from the following mathematical expression:

$$\xi = 2.44 - 1.35 \times C_{H_2SO_4} \quad (6)$$

where $C_{H_2SO_4}$ denotes the sulfuric acid concentration (mol/L) in the reactant flow supplied to the anode side.

Utilizing that mathematical expression alongside **Eq. (3)**, Fig. 6(b) graphically illustrates the decrease of the electro-osmotic water flux as the sulfuric acid concentration in the anode reactant increases for electric current densities between 0.1 and 0.8 A/cm^2. For example, supplying sulfuric acid at 0.5, 1.0, and 1.5 mol/L reduces the electro-osmotic flux of water by 9 %, 20 %, and 31 %, respectively, compared to supplying sulfuric acid at 0.1 mol/L and operating at 0.4 A/cm^2.

Fig. 6(c) compares the electro-osmotic drag coefficient estimated for the membrane of the operating electrolyzer cell used in this work to that obtained from well-representative studies, as a function of the membrane hydration number. The electro-osmotic drag coefficient estimated for the lowest sulfuric acid concentration considered (i.e., 0.1 mol/L) matches the obtained by other authors for liquid water-equilibrated membranes (i.e., $\xi \approx 2.5$ for $\lambda > 20$) [51,52], and its monotonic increase with the membrane water uptake is consistent with most prior investigations.

The electro-osmotic drag coefficient in the MCH direct electrolyzer exhibits, in general, a more pronounced decline than predicted in the literature as the water content of the membrane decreases. One plausible explanation for this finding is that a higher concentration of sulfuric acid in the anode reactant, which reduces slightly the average water content

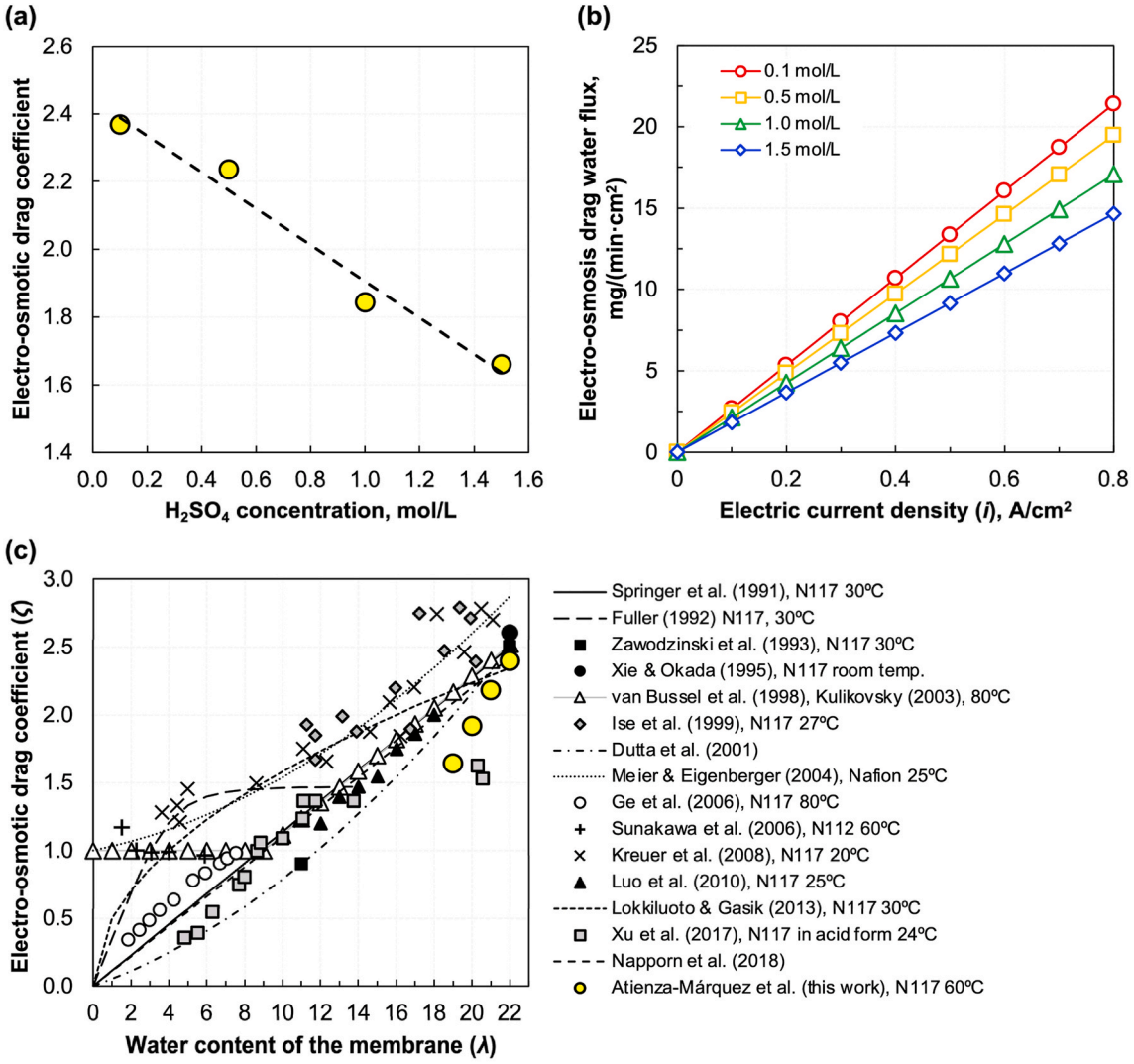

Fig. 6. (a) Electro-osmotic drag coefficient that reports the best match between the experimental water flux and the modelling outputs for electric current densities between 0.1 and 0.8 A/cm^2, operating at 60 °C. (b) Electro-osmotic water flux calculated using **Eq. (3)** with the electro-osmotic drag coefficient estimated from **Eq. (6)**. (c) Comparison of the electro-osmotic drag coefficient obtained in this study with previous values reported in the literature [31,43,46,52–62].

Table 2
Calculated and measured water flux and modeling parameters for the best fit.

Sulfuric acid in anode reactant, mol/L	Case*	Net water flux, mg/(min·cm^2)						Fitting parameters		*NMBE* (Eq. (5))
		Electric current density, A/cm^2						Electro-osmotic drag coefficient	Diffusive water flux, mg/(min·cm^2)	
		0.1	0.2	0.3	0.4	0.6	0.8			
0.1	C	2.54	5.22	7.90	10.57	15.93	21.28	2.37	0.04	0.85 %
	E	2.50	5.38	7.85	10.66	15.90	20.61			
0.5	C	1.76	4.20	6.63	9.07	13.94	18.81	2.24	0.95	0.19 %
	E	1.53	4.15	6.50	9.12	14.08	18.93			
1.0	C	0.79	2.92	5.06	7.19	11.46	15.73	1.84	1.28	1.6 %
	E	0.79	2.80	4.92	7.13	11.60	15.23			
1.5	C	0.00	1.65	3.48	5.31	8.98	12.65	1.66	1.98	−3.4 %
	E	0.44	1.73	3.48	5.48	9.17	12.89			

* Nomenclature. E: Experimental measurement (the average water flux was considered when measurements at 10% and 100% were available for a given current density). C: Calculated according to the modelling approach presented in Section 2.2.

of the membrane (Table A.1), may lead to an increased presence of sulfate ions in the membrane. This may cause more water molecules to remain attached to sulfate ions, which reduces the number of hydronium ions (H_3O^+, water molecules associated with each solvated proton) moving across the membrane, thus reducing the transport of protons via the "vehicle mechanism [63]". Consequently, less water might be dragged across the membrane towards the cathode. Furthermore, the membrane in the MCH direct electrolyzer is liquid equilibrated and exhibits high hydration levels ($\lambda \approx 18$–22) for the entire sulfuric acid concentration range investigated. This may promote proton dissociation and mobility, enabling them to hop from one water molecule to the next inside the membrane (Grotthuss hopping mechanism [64]), leading to a structural diffusion that does not involve the bulk flow of water across the membrane.

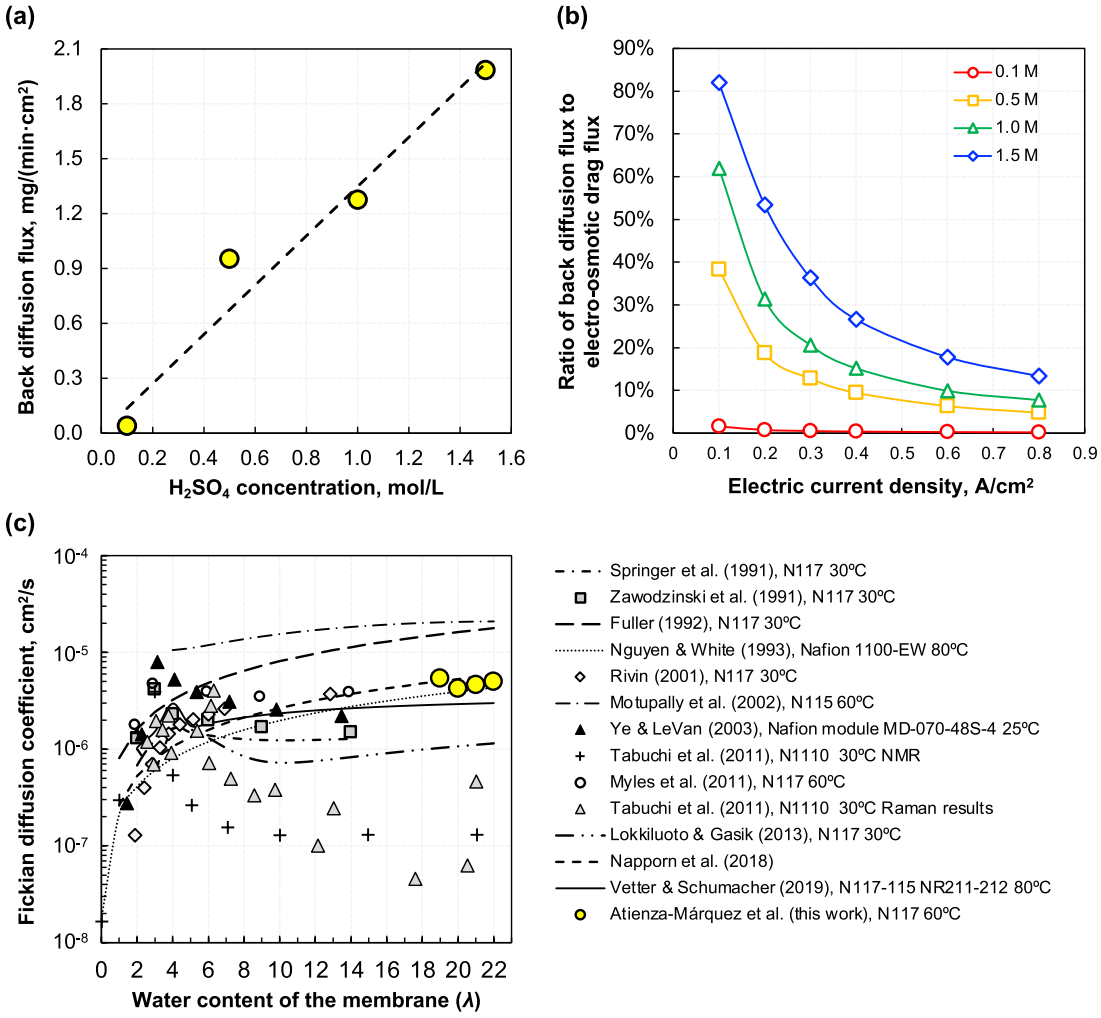

Fig. 7. (a) Back-diffusion flux that reports the best match between the experimental water flux and the modelling outputs for electric current densities between 0.1 and 0.8 A/cm^2, operating at 60 °C. (b) Share of the back diffusion flux to the total water dragged through the membrane of the electrolyzer cell for electric current densities between 0.1 and 0.8 A/cm^2. (c) Comparison of the Fickian diffusion coefficient obtained with previous literature [46,53,61,62,65–72].

3.3. Back diffusion mechanism

Fig. 7(a) and Table 2 show the value of the back diffusion water flux that minimizes the deviation between the calculated and experimentally measured net water flux across the Nafion™ membrane. The results indicate a roughly linear increase in the back diffusion flux with added sulfuric acid in the anode-side reactant. For example, the back diffusion flux increases from 1.28 to 1.98 mg/(min·cm^2) (i.e., by ~55 %) when the sulfuric acid concentration increases from 1.0 to 1.5 mol/L.

The back diffusion flux, in mg/(min·cm^2), can be estimated from the following mathematical expression as a function of the anode sulfuric acid concentration:

$$N_{w,DIF} = 1.348 \times C_{H_2SO_4} \quad (7)$$

The lower water content in the membrane at the anode side compared to the cathode side (see Table A.1) results in a back diffusion flux of water opposite to the electro-osmotic drag flux. As shown in Fig. 7 (b), this back diffusion significantly affected the net water transport, especially when the cell operates at low electric current densities and with higher concentrations of sulfuric acid in the anode reactant. At a concentration of 0.1 mol/L, the diffusion mechanism's significance is almost negligible. However, its magnitude is substantial at anode sulfuric acid concentrations of 0.5, 1.0, and 1.5 mol/L and at low current densities, representing more than 10 %, 20 %, or 30 % of the electro-osmotic flux, respectively, at electric current densities below 0.4 A/cm^2. Nonetheless, as the operating electric current increases, the impact of diffusion on the net flux decreases and becomes less significant compared to the electro-osmotic flux, even when the anode's sulfuric acid concentration was 1.5 mol/L.

Fig. 7(c) compares the steady-state Fickian diffusion coefficients obtained in this work (calculated from the hydration numbers given in Table A.1) with values reported in other studies related to Nafion™ membranes as a function of the hydration number. Reported diffusivity values for perfluorinated sulfonic-acid membranes exhibit a wide range, spanning between four orders of magnitude. In the case of the membrane used in the electrolyzer cell explored in this research, diffusivity coefficients are estimated at approximately 4-5 $\times$ 10^{-6} cm^2/s, as determined from **Eq. (4)** and the hydration numbers outlined in Table A.1. These values fall within the range displayed in Fig. 7(c), thus are consistent with diffusivity predictions from prominent studies that focus on water diffusion in Nafion™ membranes.

4. Conclusions

This paper investigated water mass transport through the polymer electrolyte membrane of an operating direct methylcyclohexane electrolyzer. The following conclusions can be drawn:

- The amount of water dragged from the anode to the cathode across the membrane increased with electric current. Electro-osmosis became the dominant water transport mechanism at high currents, while diffusion was significant at low currents. The concentration of toluene in the cathode reactant had a negligible impact on water transport across the Nafion™ membrane.
- Using diluted sulfuric acid as an anode reactant reduced water transport across the membrane and provided a degree of control over this variable. Increasing sulfuric acid concentration enhanced the back-diffusion mechanism due to the larger water concentration gradient between the two sides of the membrane, which will have a positive impact on toluene conversion efficiency. In contrast, the electro-osmotic effect was likely reduced by the larger number of sulfate ions in the membrane, thereby decreasing the number of water molecules associated with each proton moving across.
- Despite the complexity of water transport in perfluorinated sulfonic-acid membranes, the calculations based on the simplified modeling approach presented in this study demonstrated strong agreement with experimental data. The estimated electro-osmotic and diffusion coefficients were also consistent with values reported in the literature.

Because water drag across the membrane is a critical performance limitation, the results of this study will aid engineers and researchers in enhancing the design and optimizing the performance of toluene direct electro-hydrogenation electrolyzers. Future work will explore using different membranes and anode configurations to control water drag.

CRediT authorship contribution statement

Antonio Atienza-Márquez: Conceptualization, Formal analysis, Investigation, Methodology, Software, Validation, Visualization, Writing – original draft, Writing – review & editing. **Shota Oi:** Data curation, Investigation, Resources. **Takuto Araki:** Conceptualization, Methodology, Resources, Supervision. **Shigenori Mitsushima:** Conceptualization, Funding acquisition, Project administration, Supervision.

Declaration of competing interest

The authors declare that they have no known competing financial interests or personal relationships that could have appeared to influence the work reported in this paper.

Data availability

Data will be made available on request.

Acknowledgments

This study was based on results obtained from the Development of Fundamental Technology for Advancement of Water Electrolysis Hydrogen Production in Advancement of Hydrogen Technologies and Utilization Project (P14021) commissioned by the New Energy and Industrial Technology Development Organization (NEDO). The authors would like to express their gratitude to Ms. R. Shinohara and Ms. K. Ikegami for their support during the experimental phase, and to Ms. F.I. Reyna-Peña for her contributions in providing references during the initial stages of the study. Funding for open access charge: Universidad de Málaga / CBUA.

Appendix A. Water activity at the membrane

Numerous authors have developed correlations to calculate λ as a function of the thermodynamic activity of water (a_w) in water vapor-equilibrated membranes, for example, based on polynomial fits to experimental data [46,73]. Yet there is a significant disparity between them across the entire activity range. As highlighted by the water isotherms depicted in Fig. A.1 (a), these differences become particularly pronounced when approaching saturation, due to puzzling features of PFSA membranes such as Nafion and complex and controversial phenomena like Schroeder's paradox [74], which indicates that polymers absorbs more water when equilibrated in the liquid phase compared to the saturated vapor phase [75]. The complex and controversial remains unresolved, with no consensus among scholars [76]; some results prove Schroeder's Paradox, while others defend its absence.

Figure A.1 (b) also shows that liquid water-equilibrated membranes and sulfuric acid-equilibrated membranes have similar hydration numbers. However, vapor-equilibrated membranes have lower water uptake than sulfuric acid solutions, which are liquid over the entire thermodynamic activity range. This paper calculates the water content using the water uptake isotherm proposed by Tang et al. [77], which was specifically developed for membranes equilibrated with diluted sulfuric acid solutions at various concentrations.

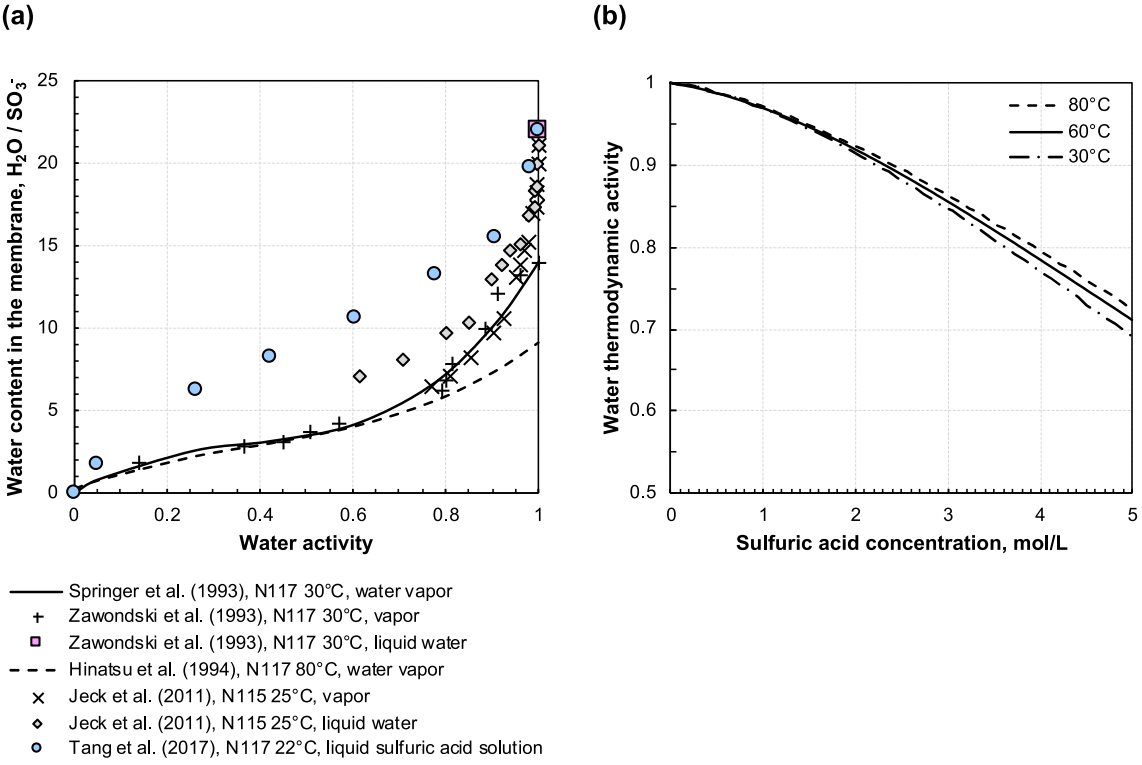

Fig. A.1. (a) Water uptake isotherms for PFSA membranes, developed for sulfuric acid solution-equilibrated membranes (Tang et al. [77]) and liquid/vapor-equilibrated membranes [46,52,73,76]. (b) Water activity for sulfuric acid solutions developed by Zhang et al. [78] and based on the NRTL molecular activity model. The shaded area represents the sulfuric acid concentration range used in this study.

The thermodynamic activity of water was determined based on the concentration of sulfuric acid. This calculation relies on the model established by Zhang et al. [78], which is graphically represented in Fig. A.1 (b) as a function of the sulfuric acid concentration. In the range of sulfuric acid concentrations considered in this work (shaded area) the water activity is barely affected by the operating temperature.

Table A.1 presents the calculated water activity and hydration number for each scenario in this study, determined by the sulfuric acid concentration in the anode reactant.

Appendix B. Polarization curves

Figure B.1. Shows the polarization curves obtained by chronoamperometry.

Table A.1
Activity of water and water content of the membrane.

Sulfuric acid in anode reactant, mol/L	Thermodynamic activity of water (a_w)[a]		Water content of the membrane (λ)[c], mol H_2O/mol SO_3^-			
	Anode ($a_{w,a}$)	Cathode ($a_{w,c}$)[b]	Anode ($\lambda_{x=0}$)	Cathode ($\lambda_{x=\delta}$)[b]	$\bar{\lambda}$	$\Delta\lambda$
0.1	0.9981	0.9998	21.74	21.98	21.86	0.23
0.5	0.9879	0.9991	20.41	21.88	21.14	1.47
1.0	0.9704	0.9981	19.05	21.74	20.40	2.69
1.5	0.9481	0.9970	17.86	21.60	19.73	3.74

[a]Calculated from the activity model for sulfuric acid solutions published in Zhang et al. [78].
[b]Calculated by assuming a 1/10 crossover of sulfuric acid from the anode reactant to the cathode side (Fig. 5(b)).
[c]Based on the water uptake isotherms developed by Tang et al. [77].

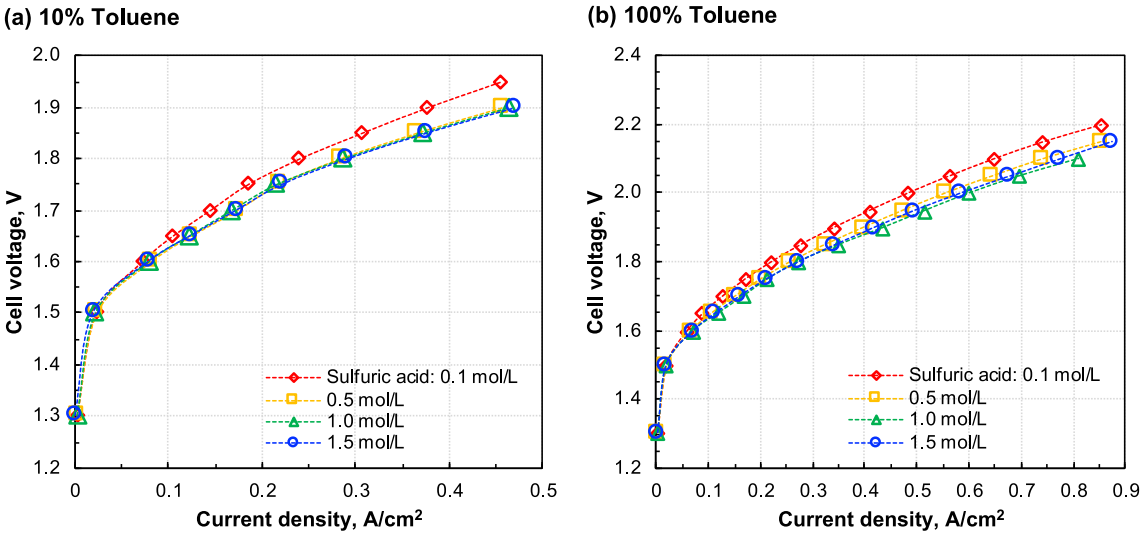

Fig. B.1. Cell voltage as a function of the current density for various sulfuric acid concentrations in the anode reactant. Toluene supply (cathode), ratio to MCH: (a) 10 %, (b) 100 %.

References

[1] Göke L, Weibezahn J, Kendziorski M. How flexible electrification can integrate fluctuating renewables. Energy 2023;278:127832. https://doi.org/10.1016/j.energy.2023.127832.

[2] d'Amore-Domenech R, Meca VL, Pollet BG, Leo TJ. On the bulk transport of green hydrogen at sea: Comparison between submarine pipeline and compressed and liquefied transport by ship. Energy 2023;267:126621. https://doi.org/10.1016/j.energy.2023.126621.

[3] Niermann M, Beckendorff A, Kaltschmitt M, Bonhoff K. Liquid organic hydrogen carrier (LOHC) – assessment based on chemical and economic properties. Int J Hydrogen Energy 2019;44:6631–54. https://doi.org/10.1016/j.ijhydene.2019.01.199.

[4] Chu C, Wu K, Luo B, Cao Q, Zhang H. Hydrogen storage by liquid organic hydrogen carriers: catalyst, renewable carrier, and technology – a review. Carbon Resources Conversion 2023;6:334–51. https://doi.org/10.1016/j.crcon.2023.03.007.

[5] Sharma P, Bera T, Semwal K, Badhe RM, Sharma A, Ramakumar SSV, et al. Theoretical analysis of design of filament wound type 3 composite cylinder for the storage of compressed hydrogen gas. Int J Hydrogen Energy 2020;45:25386–97. https://doi.org/10.1016/j.ijhydene.2020.06.269.

[6] Bi Y, Ju Y. Design and analysis of an efficient hydrogen liquefaction process based on helium reverse Brayton cycle integrating with steam methane reforming and liquefied natural gas cold energy utilization. Energy 2022;252:124047. https://doi.org/10.1016/j.energy.2022.124047.

[7] Kumar A, Muthukumar P. Experimental investigation on the poisoning characteristics of methane as impurity in La0.9Ce0.1Ni5 based hydrogen storage and purification system. Energy 2022;259:124888. https://doi.org/10.1016/j.energy.2022.124888.

[8] Kannaiyan K, Lekshmi GS, Ramakrishna S, Kang M, Kumaravel V. Perspectives for the green hydrogen energy-based economy. Energy 2023;284:129358. https://doi.org/10.1016/j.energy.2023.129358.

[9] Abdin Z, Tang C, Liu Y, Catchpole K. Large-scale stationary hydrogen storage via liquid organic hydrogen carriers. iScience 2021;24:102966. https://doi.org/10.1016/j.isci.2021.102966.

[10] Hunt JD, Nascimento A, Zakeri B, Barbosa PSF. Hydrogen Deep Ocean Link: a global sustainable interconnected energy grid. Energy 2022;249:123660. https://doi.org/10.1016/j.energy.2022.123660.

[11] Godinho J, Hoefnagels R, Braz CG, Sousa AM, Granjo JFO. An economic and greenhouse gas footprint assessment of international maritime transportation of hydrogen using liquid organic hydrogen carriers. Energy 2023;278:127673. https://doi.org/10.1016/j.energy.2023.127673.

[12] International Energy Agency (IEA). Global hydrogen review. 2023.

[13] Beckmann J, Klöckner K, Letmathe P. Scenario-based multi-criteria evaluation of sector coupling-based technology pathways for decarbonization with varying degrees of disruption. Energy 2024;297:131248. https://doi.org/10.1016/j.energy.2024.131248.

[14] Reyna-Peña FI, Atienza-Márquez A, Jang S, Shiono R, Shigemasa K, Araki T, et al. In situ X-ray CT visualization of hydrogen bubbles inside the porous transport layer of a direct toluene electro-hydrogenation electrolyzer. Int J Hydrogen Energy 2024;50:787–98. https://doi.org/10.1016/j.ijhydene.2023.08.132.

[15] Zhang C, Song P, Zhang Y, Xiao L, Hou J, Wang X. Technical and cost analysis of imported hydrogen based on MCH-TOL hydrogen storage technology. Int J Hydrogen Energy 2022;47:27717–32. https://doi.org/10.1016/j.ijhydene.2022.06.113.

[16] Markiewicz M, Zhang Y-Q, Empl MT, Lykaki M, Thöming J, Steinberg P, et al. Hazard assessment of quinaldine-, alkylcarbazole-, benzene- and toluene-based liquid organic hydrogen carrier (LOHCs) systems. Energy Environ Sci 2019;12:366–83. https://doi.org/10.1039/C8EE01696H.

[17] Wijayanta AT, Oda T, Purnomo CW, Kashiwagi T, Aziz M. Liquid hydrogen, methylcyclohexane, and ammonia as potential hydrogen storage: Comparison review. Int J Hydrogen Energy 2019;44:15026–44. https://doi.org/10.1016/j.ijhydene.2019.04.112.

[18] Shigemasa K, Atienza-Márquez A, Inoue K, Jang S, Peña FIR, Araki T, et al. Visualization of dragged water and generated hydrogen bubbles in a direct toluene electro-hydrogenation electrolyzer. J Power Sources 2023;554:232304. https://doi.org/10.1016/j.jpowsour.2022.232304.

[19] Nagasawa K, Kato A, Nishiki Y, Matsumura Y, Atobe M, Mitsushima S. The effect of flow-field structure in toluene hydrogenation electrolyzer for energy carrier synthesis system. Electrochim Acta 2017;246:459–65. https://doi.org/10.1016/j.electacta.2017.06.081.

[20] Nagasawa K, Sugita Y, Atienza-Márquez A, Kuroda Y, Mitsushima S. Effect of the cathode catalyst loading on mass transfer in toluene direct electrohydrogenation. J Electroanal Chem 2023;938:117431. https://doi.org/10.1016/j.jelechem.2023.117431.

[21] Nagasawa K, Tanimoto K, Koike J, Ikegami K, Mitsushima S. Toluene permeation through solid polymer electrolyte during toluene direct electro-hydrogenation for energy carrier synthesis. J Power Sources 2019;439:227070. https://doi.org/10.1016/j.jpowsour.2019.227070.

[22] Nagasawa K, Mitsushima S. Electrolyzer technologies in toluene direct electro-hydrogenation for methylcyclohexane synthesis. J Jpn Petrol Inst 2024;67:97–104. https://doi.org/10.1627/jpi.67.97.

[23] Nagasawa K, Sawaguchi Y, Kato A, Nishiki Y, Mitsushima S. Rate-determining factor of the performance for toluene electrohydrogenation electrolyzer. Electrocatalysis 2017;8:164–9. https://doi.org/10.1007/s12678-017-0351-4.

[24] Nagasawa K, Sawaguchi Y, Kato A, Nishiki Y, Mitsushima S. Chemical-hydrogenation Functionalized flow-field in toluene direct electro-hydrogenation electrolyzer for energy-carrier synthesis system. Electrochemistry 2018;86:339–44. https://doi.org/10.5796/electrochemistry.18-00055.

[25] Mitsushima S, Takakuwa Y, Nagasawa K, Sawaguchi Y, Kohno Y, Matsuzawa K, et al. Membrane electrolysis of toluene hydrogenation with water decomposition for energy carrier synthesis. Electrocatalysis 2016;7:127–31. https://doi.org/10.1007/s12678-015-0289-3.

[26] ENEOS Corporation. Direct MCH® ENEOS; 2024. https://www.eneos.co.jp/english/company/rd/intro/low_carbon/ems.html. [Accessed 3 May 2024].

[27] ENEOS. Australian Demonstration Plant Begins operation toward the Development of a CO2-free Hydrogen Supply Chain n.d. https://www.eneos.co.jp/english/newsrelease/2022/pdf/20230130_01.pdf.

[28] Majsztrik P, Bocarsly A, Benziger J. Water permeation through nafion membranes: the role of water activity. J Phys Chem B 2008;112:16280–9. https://doi.org/10.1021/jp804197x.

[29] Park J, Kwon O, Oh H-M, Jeong S, So Y, Park G, et al. Optimizing design of catalyst layer structure with carbon-supported platinum weight ratio mixing method for proton exchange membrane fuel cells. Energy 2024;291:130363. https://doi.org/10.1016/j.energy.2024.130363.

[30] Li F, Cai S, Li S, Luo X, Tu Z. Pore-scale study of water and mass transport characteristic in anion exchange membrane fuel cells with anisotropic gas diffusion layer. Energy 2024;293:130599. https://doi.org/10.1016/j.energy.2024.130599.

[31] Xu F, Leclerc S, Stemmelen D, Perrin J-C, Retournard A, Canet D. Study of electro-osmotic drag coefficients in Nafion membrane in acid, sodium and potassium forms

by electrophoresis NMR. J Membr Sci 2017;536:116–22. https://doi.org/10.1016/j.memsci.2017.04.067.
[32] Kusoglu A, Weber AZ. New insights into perfluorinated sulfonic-acid ionomers. Chem Rev 2017;117:987–1104. https://doi.org/10.1021/acs.chemrev.6b00159.
[33] Vetter R, Schumacher JO. Experimental parameter uncertainty in proton exchange membrane fuel cell modeling. Part I: scatter in material parameterization. J Power Sources 2019;438:227018. https://doi.org/10.1016/j.jpowsour.2019.227018.
[34] Katsounaros I, Cherevko S, Zeradjanin AR, Mayrhofer KJJ. Oxygen electrochemistry as a cornerstone for sustainable energy conversion. Angew Chem Int Ed 2014;53:102–21. https://doi.org/10.1002/anie.201306588.
[35] Hu JM, Meng HM, Zhang JQ, Cao CN. Degradation mechanism of long service life Ti/IrO2–Ta2O5 oxide anodes in sulphuric acid. Corrosion Sci 2002;44:1655–68. https://doi.org/10.1016/S0010-938X(01)00165-2.
[36] De Nora Permelec Ltd Fujisawa. DSE® electrode for Functional Water n.d. https://japan.denora.com/products/DSE–electrode-for-Functional-Water.html accessed October 25, 2023).
[37] SGL Carbon. SIGRACET® Fuel Cell Components n.d. https://www.sglcarbon.com/en/markets-solutions/material/sigracet-fuel-cell-components/(accessed October 25, 2023).
[38] Tanaka Holdings Co., Ltd. Precious Metals PEFCs Electrode Catalyst n.d. https://tanaka-preciousmetals.com/jp/products/detail/pefcs/(accessed October 25, 2023).
[39] Python 3.12.0. 2023.
[40] Bernardi DM, Verbrugge MW. A mathematical model of the solid-polymer-electrolyte fuel cell. J Electrochem Soc 1992;139:2477–91. https://doi.org/10.1149/1.2221251.
[41] Barragán VM, Kjelstrup S. Thermo-osmosis in membrane systems: a review. J Non-Equilibrium Thermodyn 2017;42. https://doi.org/10.1515/jnet-2016-0088.
[42] Hu J, Li J, Xu L, Huang F, Ouyang M. Analytical calculation and evaluation of water transport through a proton exchange membrane fuel cell based on a one-dimensional model. Energy 2016;111:869–83. https://doi.org/10.1016/j.energy.2016.06.020.
[43] Ge S, Yi B, Ming P. Experimental determination of electro-osmotic drag coefficient in nafion membrane for fuel cells. J Electrochem Soc 2006;153:A1443. https://doi.org/10.1149/1.2203934.
[44] Jiao K, Li X. Water transport in polymer electrolyte membrane fuel cells. Prog Energy Combust Sci 2011;37:221–91. https://doi.org/10.1016/j.pecs.2010.06.002.
[45] Sellin RC, Mozet K, Ménage A, Dillet J, Didierjean S, Maranzana G. Measuring electro-osmotic drag coefficients in PFSA membranes without any diffusion assumption. Int J Hydrogen Energy 2019;44:24905–12. https://doi.org/10.1016/j.ijhydene.2019.07.076.
[46] Springer TE, Zawodzinski TA, Gottesfeld S. Polymer electrolyte fuel cell model. J Electrochem Soc 1991;138:2334–42. https://doi.org/10.1149/1.2085971.
[47] Ge S, Li X, Yi B, Hsing I-M. Absorption, desorption, and transport of water in polymer electrolyte membranes for fuel cells. J Electrochem Soc 2005;152:A1149. https://doi.org/10.1149/1.1899263.
[48] Chen L, Chen Y, Tao W-Q. Schroeder's paradox in proton exchange membrane fuel cells: a review. Renew Sustain Energy Rev 2023;173:113050. https://doi.org/10.1016/j.rser.2022.113050.
[49] Chupin S, Colinart T, Didierjean S, Dubé Y, Agbossou K, Maranzana G, et al. Numerical investigation of the impact of gas and cooling flow configurations on current and water distributions in a polymer membrane fuel cell through a pseudo-two-dimensional diphasic model. J Power Sources 2010;195:5213–27. https://doi.org/10.1016/j.jpowsour.2010.03.027.
[50] Majsztrik PW, Satterfield MB, Bocarsly AB, Benziger JB. Water sorption, desorption and transport in Nafion membranes. J Membr Sci 2007;301:93–106. https://doi.org/10.1016/j.memsci.2007.06.022.
[51] Xie G, Okada T. Water transport behavior in nafion 117 membranes. J Electrochem Soc 1995;142:3057–62. https://doi.org/10.1149/1.2048686.
[52] Zawodzinski TA, Derouin C, Radzinski S, Sherman RJ, Smith VT, Springer TE, et al. Water uptake by and transport through Nafion® 117 membranes. J Electrochem Soc 1993;140:1041–7. https://doi.org/10.1149/1.2056194.
[53] Fuller TF. Departmem of chemical engineering university of California and n.d.
[54] Van Bussel HPLH, Koene FGH, Mallant RKAM. Dynamic model of solid polymer fuel cell water management. J Power Sources 1998;71:218–22. https://doi.org/10.1016/S0378-7753(97)02744-4.
[55] Ise M, Kreuer KD, Maier J. Electroosmotic drag in polymer electrolyte membranes: an electrophoretic NMR study. Solid State Ionics 1999;125:213–23. https://doi.org/10.1016/S0167-2738(99)00178-2.
[56] Dutta S, Shimpalee S, Van Zee JW. Numerical prediction of mass-exchange between cathode and anode channels in a PEM fuel cell. Int J Heat Mass Tran 2001;44:2029–42. https://doi.org/10.1016/S0017-9310(00)00257-X.
[57] Kulikovsky AA. Quasi-3D modeling of water transport in polymer electrolyte fuel cells. J Electrochem Soc 2003;150:A1432. https://doi.org/10.1149/1.1611489.
[58] Meier F, Eigenberger G. Transport parameters for the modelling of water transport in ionomer membranes for PEM-fuel cells. Electrochim Acta 2004;49:1731–42. https://doi.org/10.1016/j.electacta.2003.12.004.
[59] Sunakawa D, Oyama S, Araki T, Onda K. Measurement of diffusion coefficient and electro-osmotic coefficient of water at PEFC. Electrochemistry 2006;74:732–6. https://doi.org/10.5796/electrochemistry.74.732.
[60] Kreuer KD, Schuster M, Obliers B, Diat O, Traub U, Fuchs A, et al. Short-side-chain proton conducting perfluorosulfonic acid ionomers: why they perform better in PEM fuel cells. J Power Sources 2008;178:499–509. https://doi.org/10.1016/j.jpowsour.2007.11.011.
[61] Lokkiluoto A, Gasik MM. Modeling and experimental assessment of Nafion membrane properties used in SO2 depolarized water electrolysis for hydrogen production. Int J Hydrogen Energy 2013;38:10–9. https://doi.org/10.1016/j.ijhydene.2012.09.168.
[62] Napporn TW, Karpenko-Jereb L, Pichler B, Hacker V. Polymer electrolyte fuel cells. Fuel cells and hydrogen. Elsevier; 2018. p. 63–89. https://doi.org/10.1016/B978-0-12-811459-9.00004-9.
[63] Kreuer K, Rabenau A, Weppner W. Vehicle mechanism, A New model for the interpretation of the conductivity of fast proton conductors. Angew Chem Int Ed Engl 1982;21:208–9. https://doi.org/10.1002/anie.198202082.
[64] Agmon N. The Grotthuss mechanism. Chem Phys Lett 1995;244:456–62. https://doi.org/10.1016/0009-2614(95)00905-J.
[65] Zawodzinski TA, Neeman M, Cottesfeld S. Determination of water dlffusion coefficients in perfluorosulfonate ionomeric membranes. Am Chem Soc 1991;95:6040–4.
[66] Zawodzinskijr T, Springer T, Uribe F, Gottesfeld S. Characterization of polymer electrolytes for fuel cell applications. Solid State Ionics 1993;60:199–211. https://doi.org/10.1016/0167-2738(93)90295-E.
[67] Nguyen TV, White RE. A water and heat management model for proton-exchange-membrane fuel cells. J Electrochem Soc 1993;140:2178–86. https://doi.org/10.1149/1.2220792.
[68] Motupally S, Becker AJ, Weidner JW. Water transport in polymer electrolyte membrane electrolyzers used to recycle anhydrous HCl. J Electrochem Soc 2002;149:D63–71.
[69] Ye X, Douglas LeVan M. Water transport properties of Nafion membranes. J Membr Sci 2003;221:147–61. https://doi.org/10.1016/S0376-7388(03)00255-2.
[70] Tabuchi Y, Ito R, Tsushima S, Hirai S. Analysis of in situ water transport in Nafion® by confocal micro-Raman spectroscopy. J Power Sources 2011;196:652–8. https://doi.org/10.1016/j.jpowsour.2010.07.078.
[71] Myles TD, Kiss AM, Grew KN, Peracchio AA, Nelson GJ, Chiu WKS. Calculation of water diffusion coefficients in an anion exchange membrane using a water permeation technique. J Electrochem Soc 2011;158:B790. https://doi.org/10.1149/1.3585834.
[72] Vetter R, Schumacher JO. Free open reference implementation of a two-phase PEM fuel cell model. Comput Phys Commun 2019;234:223–34. https://doi.org/10.1016/j.cpc.2018.07.023.
[73] Hinatsu JT, Mizuhata M, Takenaka H. Water uptake of perfluorosulfonic acid membranes from liquid water and water vapor. J Electrochem Soc 1994;141:1493–8. https://doi.org/10.1149/1.2054951.
[74] Bass M, Berman A, Singh A, Konovalov O, Freger V. Surface structure of nafion in vapor and liquid. J Phys Chem B 2010;114:3784–90. https://doi.org/10.1021/jp9113128.
[75] Freger V. Hydration of ionomers and schroeder's paradox in Nafion. J Phys Chem B 2009;113:24–36. https://doi.org/10.1021/jp806326a.
[76] Jeck S, Scharfer P, Kind M. Absence of Schroeder's paradox: experimental evidence for water-swollen Nafion® membranes. J Membr Sci 2011;373:74–9. https://doi.org/10.1016/j.memsci.2011.02.036.
[77] Tang Z, Svoboda R, Lawton JS, Aaron DS, Papandrew AB, Zawodzinski TA. Composition and conductivity of membranes equilibrated with solutions of sulfuric acid and vanadyl sulfate. J Electrochem Soc 2013;160:F1040–7. https://doi.org/10.1149/2.083309jes.
[78] Zhang L, Grace PM, Sun D-W. An accurate water activity model for sulfuric acid solutions and its implementation on moisture sorption isotherm determination. Dry Technol 2022;40:2540–9. https://doi.org/10.1080/07373937.2020.1869037.